

## An $S = 6$ Cyanide-Bridged Octanuclear $\text{Fe}^{\text{III}}_4\text{Ni}^{\text{II}}_4$ Complex that Exhibits Slow Relaxation of the Magnetization

Dongfeng Li,<sup>†</sup> Sean Parkin,<sup>†</sup> Guangbin Wang,<sup>‡</sup> Gordon T. Yee,<sup>‡</sup> Rodolphe Clérac,<sup>\*,§</sup>  
Wolfgang Wernsdorfer,<sup>||</sup> and Stephen M. Holmes<sup>\*,†</sup>

Department of Chemistry, University of Kentucky, Lexington, Kentucky 40506-0055, Department of Chemistry, Virginia Polytechnic Institute and State University, Blacksburg, Virginia 24061, Centre de Recherche Paul Pascal, UPR-CNRS 8641, 115 avenue du Dr. A. Schweitzer, 33600 Pessac, France, and Laboratoire Louis Néel, CNRS, BP-166, 38042 Grenoble Cedex 9, France

Received January 17, 2006; E-mail: smholm2@uky.edu; clerac@crpp-bordeaux.cnrs.fr

The study of single-molecule magnets (SMMs) has remained an active arena of research over the past decade.<sup>1</sup> The most celebrated example is  $\text{Mn}_{12}\text{O}_{12}(\text{O}_2\text{CMe})_{16}(\text{OH}_2)_4$ , which exhibits superparamagnetic-like behavior owing to the large-spin ground state ( $S = 10$ ) and uniaxial anisotropy ( $D < 0$  and small  $E$ ) derived from the transition metal centers present.<sup>1</sup> These characteristics create an energy barrier ( $\Delta$ ) between two thermodynamically equivalent  $m_S = \pm S$  configurations. Below  $T_B$ , the so-called “blocking temperature”, the available thermal energy is insufficient to overcome  $\Delta$ , and the spin is trapped in one of two possible configurations. Application of large magnetic fields ( $H$ ) saturate the magnetization ( $M$ ) of the sample, and upon removal of this field ( $H = 0$ ), a slow decay of  $M$  toward zero with a characteristic relaxation time ( $\tau$ ) is observed. The relaxation time usually exhibits thermally activated behavior and can be measured via magnetization ( $M$ ) vs time or frequency ( $\nu$ ) dependence of the ac susceptibility, respectively; at very low temperatures, quantum tunneling of the magnetization (QTM) often relaxes the magnetization faster than thermally activated pathways.<sup>1,2</sup>

Recently, we described the preparation of several SMMs derived from tris(pyrazolyl)borate tricyanometalates.<sup>2a,f</sup> Poly(pyrazolyl)borates are useful ancillary ligands for constructing polynuclear magnetic complexes that exhibit tunable magnetic and optical properties.<sup>2a,c,f,i</sup> Facile chemical modification of the pyrazolylborate framework at up to 10 substitutable positions, allows for the systematic alteration of coordination preferences, functional groups, and electronic properties of derived complexes.<sup>3a</sup> Via a building block synthetic approach, poly(pyrazolyl)borate cyanometalates are allowed to self-assemble into discrete clusters whose properties are derived from the metal centers utilized. This synthetic approach allows for the systematic insertion of metal centers into a given structural archetype and structure–property relationships to be ascertained.<sup>2</sup>

As part of a continuing effort to prepare magnetic and photo-magnetic cyanometalate clusters, a series of functionalized tris(pyrazolyl)borate and -methane ligands and their cubic  $\text{Fe}^{\text{III}}_4\text{Ni}^{\text{II}}_4$  cyanometalate cluster derivatives have been prepared, to probe possible relationships between molecular symmetry and blocking temperatures, within a given structural archetype.<sup>2h</sup> In the present communication, we report the synthetic, spectroscopic, structural, and magnetic properties of an octanuclear complex that exhibits an  $S = 6$  ground state and slow relaxation of the magnetization.

Treatment of  $[\text{NEt}_4][(\text{pzTp})\text{Fe}^{\text{III}}(\text{CN})_3]$  (pzTp = tetra(pyrazol-1-yl)borate) with nickel(II) trifluoromethanesulfonate in

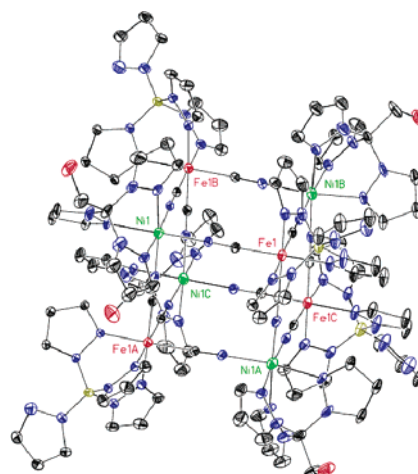


**Figure 1.** X-ray structure of **1**. Thermal ellipsoids are at the 30% level, and all anions, lattice solvent, and hydrogen atoms are removed for clarity. Selected bond distances (Å) and angles (deg): Fe1–C13 1.926(7), Fe1–N1 1.977(6), Ni1–N15 2.060(6); C13–Fe1–C15 88.0(3), N15–Ni1–N16 92.9(2).

DMF, followed by excess 2,2,2-tris(pyrazolyl)ethanol ( $\text{L}$ )<sup>3b</sup> in  $\text{CH}_2\text{Cl}_2$ , affords dark-red crystals of  $[(\text{pzTp})\text{Fe}^{\text{III}}(\text{CN})_3]_4[\text{Ni}^{\text{II}}\text{L}]_4[\text{OTf}]_4 \cdot 10\text{DMF} \cdot \text{Et}_2\text{O}$  (**1**) within several days.<sup>2g</sup> The infrared spectrum of **1** exhibits an intense  $\nu_{\text{CN}}$  stretching absorption at  $2174\text{ cm}^{-1}$  that is shifted to higher energy relative to  $[\text{NEt}_4][(\text{pzTp})\text{Fe}^{\text{III}}(\text{CN})_3]$  ( $2120\text{ cm}^{-1}$ ), suggesting that bridging cyanides are present.<sup>2a,f–i</sup>

Compound **1** crystallizes as a cationic octanuclear  $\text{Fe}^{\text{III}}_4\text{Ni}^{\text{II}}_4$  complex in the tetragonal ( $I4_1/acd$ ) space group.<sup>2g,4</sup> Compound **1** contains  $\text{Fe}^{\text{III}}$  and  $\text{Ni}^{\text{II}}$  centers that reside in alternate corners of the distorted molecular box and are linked via cyanides into  $\text{Fe}^{\text{III}}-(\mu\text{-CN})-\text{Ni}^{\text{II}}$  units; the bridging cyanides are located on the cube edges (Figure 1). The average Fe–C and Ni–N bond distances are respectively 1.926(7) and 2.060(6) Å, while the cyanide C–Fe–C and N–Ni–N bond angles are respectively 88.0(3) and 92.9(2)°; the corresponding average edge (Fe1...Ni1), face (Fe1...Fe1A), and body diagonal (Fe1...Ni1C) distances are ca. 5.120(3), 7.364(4), and 8.858(4) Å, respectively.<sup>2g</sup>

For **1**, the  $\chi_{\text{MT}}$  vs  $T$  data suggests that the  $\text{Fe}^{\text{III}}$  and  $\text{Ni}^{\text{II}}$  centers are ferromagnetically coupled (Figure 2), since  $\chi_{\text{MT}}$  gradually increases from  $6.90\text{ cm}^3\text{ K mol}^{-1}$  (300 K), to a maximum value of  $18.9\text{ cm}^3\text{ K mol}^{-1}$  at 6.0 K. From the structure of **1**, the magnetic data has been simulated (MAGPACK)<sup>5a</sup> via the following Hamiltonian:  $H = -2J_{\text{iso}}[S_1(S_6+S_7+S_8) + S_2(S_5+S_7+S_8) + S_3(S_5+S_6+S_8) + S_4(S_5+S_6+S_7)]$ , where  $J_{\text{iso}}$  is the isotropic exchange between the low-spin  $\text{Fe}^{\text{III}}$  and  $\text{Ni}^{\text{II}}$  sites, and  $S_i$  is the spin operator for each metal center ( $S_i = 1/2$ ,  $\text{Fe}^{\text{III}}$ ,  $i = 5-8$ ;  $S_i = 1$ ,  $\text{Ni}^{\text{II}}$ ,  $i = 1-4$ ).

<sup>†</sup> University of Kentucky.

<sup>‡</sup> Virginia Polytechnic Institute and State University.

<sup>§</sup> Centre de Recherche Paul Pascal.

<sup>||</sup> Laboratoire Louis Néel.

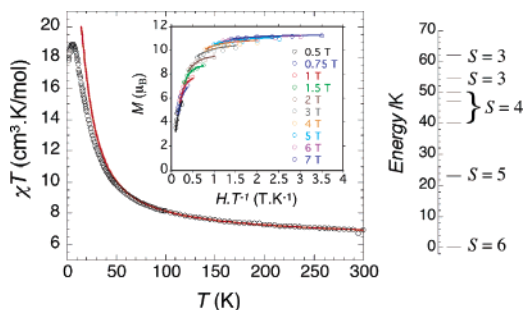


**Figure 2.**  $\chi T$  vs  $T$  plot for **1** at  $H = 0.1$  T (left). Red line: MAGPACK simulation of the data above 30 K. (Inset) Plot of reduced magnetization vs  $H/T$  between 2 and 5 K. Solid lines represent least-squares fitting of the data. Diagram of the first seven energy levels for **1** (right).

Neglecting the magnetic data below 30 K, to avoid possible effects of the magnetic ground-state anisotropy and intercluster interactions, the calculated values of  $g_{\text{iso}}$  and  $J_{\text{iso}}$  are 2.20(5) and +9.5(5) K, respectively.<sup>2g</sup> As expected for low-spin  $\text{Fe}^{\text{III}}$  ( $S = 1/2$ ) centers that exhibit orbital contributions to the magnetic moment, the  $g_{\text{iso}}$  value deviates significantly from 2.<sup>2a,5</sup> The magnitude of the magnetic exchange is comparable to several known polynuclear complexes containing  $\text{Fe}^{\text{III}}$  and  $\text{Ni}^{\text{II}}$  centers.<sup>2a,f,h-j</sup>

Considering the estimated value of  $J_{\text{iso}}$ , the first excited state ( $S = 5$ ) is ca. 23.2 K above the  $S = 6$  ground state for **1**. This ground-state energy difference is confirmed by the field dependence of the magnetization 1.85 K, since  $M$  approaches  $12 \mu_{\text{B}}$  at 7 T (Figure S5). Least-squares fitting of the  $M$  vs  $H/T$  data affords  $D/k_{\text{B}} = -0.33$  K, suggesting that the maximum SMM energy barrier is  $\Delta = |D|S_{\text{T}}^2/k_{\text{B}} = 11.9$  K (Inset of Figure 2).<sup>2g</sup>

To further probe suspected SMM behavior, the temperature dependence of the ac susceptibility was measured at various frequencies at  $H = 0$  Oe (Figures S6, S7). Compound **1** exhibits rather small frequency-independent  $\chi''$  values that are ca. 100 times smaller than  $\chi'$  (Figure S6). Initially, the small  $\chi''$  signal was attributed to an undefined magnetic species. However, the frequency dependence of  $\chi''$  at 1.8 K in the presence of nonzero  $H$  fields, suggests that **1** exhibits two intrinsic relaxation modes of significant intensity in the 1–1500 Hz frequency range (Figure S7). The origin of the two relaxation modes is unclear, but qualitatively similar behavior has been reported by Boskovic et al. for complexes of  $[\text{Mn}_4\text{Cl}_4(\text{L}')_4]$  ( $\text{H}_2\text{L}' = 4\text{-tert-butyl-salicylidene-2-ethanolamine}$ ) stoichiometry.<sup>5b</sup> We propose that crystallographic disorder, intercluster interactions, or phonon-bottleneck effects are the origin of the atypical relaxation behavior exhibited by **1**.<sup>5c</sup>

To further investigate magnetization relaxation in **1**,  $\mu$ -SQUID measurements using an oriented single crystal and application of a magnetic field ( $H$ ) along the anisotropy easy axis, were performed.<sup>6</sup> As shown in Figure 3, a butterfly-type hysteresis loop appears between 2 and 1 K (for a sweep rate of 0.14 T/s) for **1**. Consistent with the ac data, fast relaxation of the magnetization is observed when  $H = 0$ , as expected for fast ground-state quantum tunneling (Figure S6). However, in the presence of small magnetic fields ( $0 < H < 1$  T), slow relaxation of the magnetization is seen for **1** (Figures S8, S9). Furthermore, the hysteresis loops exhibited by **1** are sweep-rate dependent at 0.04 K, a property that is often observed for SMMs (Figure 3).

In summary we have described the synthesis and structural and magnetic characterizations of a cyanometalate  $S = 6$  anisotropic complex that exhibits slow field-dependent relaxation of the

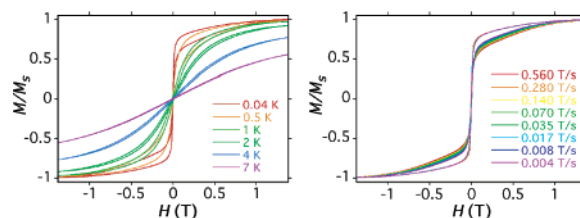


**Figure 3.**  $\mu$ -SQUID magnetization vs  $H$  measurements; (left) from 0.04 to 7 K at 0.14 T  $\text{s}^{-1}$  scan rate; (right) for different scan rates at  $T = 0.04$  K.

magnetization. We anticipate that structural distortion and insertion of more anisotropic metal centers into the cluster may ultimately afford analogues that exhibit greater total anisotropy and possibly SMM behavior at higher temperatures than **1**.

**Acknowledgment.** S.M.H. gratefully acknowledges the donors of the American Chemical Society Petroleum Research Fund (PRF 38388-G3), the Kentucky Science and Engineering Foundation (Grants KSEF-621-RDE-006 and KSEF-992-RDE-008), the University of Kentucky Summer Faculty Research Fellow, and Major Research Project programs for financial support. R.C. thanks the CNRS, the University of Bordeaux 1, and the Conseil Régional d'Aquitaine for a financial support. G.T.Y. thanks the National Science Foundation (Grant CHE-0210395) for financial support. S.M.H. is also grateful to Eugenio Coronado for providing the MAGPACK program.

**Supporting Information Available:** X-ray crystallographic data in CIF format, synthetic details, and additional magnetic data. This information is available free of charge via the Internet at <http://pubs.acs.org>.

## References

- (1) (a) Sessoli, R.; Gatteschi, D. *Angew. Chem., Int. Ed.* **2003**, *42*, 268–297 and references therein. (b) Beltran, L. M. C.; Long, J. R. *Acc. Chem. Res.* **2005**, *38*, 325–334 and references therein.
- (2) (a) Li, D.; Parkin, S.; Wang, G.; Yee, G. T.; Prosvirin, A. V.; Holmes, S. M. *Inorg. Chem.* **2005**, *44*, 4903–4905. (b) Schelter, E. J.; Prosvirin, A. V.; Dunbar, K. R. *J. Am. Chem. Soc.* **2004**, *126*, 15004–15005. (c) Wang, S.; Zou, J.-L.; Zhou, H.-C.; Choi, H. J.; Ke, Y.; Long, J. R.; You, X.-Z. *Angew. Chem., Int. Ed.* **2004**, *43*, 5940–5943. (d) Berlinguette, C. P.; Vaughn, D.; Cañada-Vilalta, C.; Galán-Mascarós, J. R.; Dunbar, K. R. *Angew. Chem., Int. Ed.* **2003**, *42*, 1523–1526. (e) Sokol, J. J.; Hee, A. G.; Long, J. R. *J. Am. Chem. Soc.* **2002**, *124*, 7656–7657. (f) Li, D.; Clerac, R.; Parkin, S.; Wang, G.; Yee, G. T.; Holmes, S. M. Manuscript submitted. (g) See Supporting Information. (h) Yang, J. Y.; Shores, M. P.; Sokol, J. J.; Long, J. R. *Inorg. Chem.* **2003**, *42*, 1403–1419. (i) Kim, J.; Han, S.; Cho, I.-K.; Choi, K. Y.; Heu, M.; Yoon, S.; Suh, B. J. *Polyhedron* **2004**, *23*, 1333–1339. (j) Li, D.; Parkin, S.; Wang, G.; Yee, G. T.; Holmes, S. M. *Inorg. Chem.* **2006**, *45*, 1951–1959.
- (3) (a) Trofimenko, S. *Scorpionates, The Coordination Chemistry of Polypyrazolylborate Ligands*; Imperial College Press: London, 1999. (b) Reger, D. L.; Grattan, T. C.; Brown, K. J.; Little, C. A.; Lamba, J. J. S.; Rheingold, A. L.; Sommer, R. D. *J. Organomet. Chem.* **2000**, *607*, 120–128.
- (4) (a) Crystal and structure refinement parameters: **1**,  $\text{C}_{142}\text{H}_{176}\text{B}_4\text{F}_{12}\text{Fe}_4\text{N}_7\text{Ni}_4\text{O}_{27}\text{S}_4$ ,  $I_4$ /acd,  $Z = 8$ ,  $a = b = 25.3637(1)$  Å,  $c = 68.0310(7)$  Å,  $V = 43765.5(5)$  Å<sup>3</sup>,  $R_1 = 0.1148$ ,  $wR_2 = 0.3821$ . All data were collected on a Bruker X8 Proteum rotating-anode CCD diffractometer with graphite-monochromated  $\text{Cu K}\alpha$  ( $\lambda = 1.54178$  Å) radiation at 90.0(2) K. The structure was solved by direct methods and refined against all data using SHELXL 97.
- (5) (a) Borrás-Almenar, J. J.; Clemente-Juan, J. M.; Coronado, E.; Tsukerblat, B. S. *J. Comput. Chem.* **2001**, *22*, 985–991. (b) Boskovic, C.; Bircher, R.; Tregenna-Piggott, P. L. W.; Güdel, H.; Paulsen, C.; Wernsdorfer, W.; Barra, A. L.; Khatsko, E.; Neels, A.; Stoeckli-Evans, H. *J. Am. Chem. Soc.* **2003**, *125*, 14046–14058. (c) Chakov, N. E.; Wernsdorfer, W.; Abboud, K. A.; Christou, G. *Inorg. Chem.* **2004**, *43*, 5919–5930.
- (6) Wernsdorfer, W. *Adv. Chem. Phys.* **2001**, *118*, 99–190.

JA058626I